Chapter 4

POLARIZATION CONTROL OF MORPHOLOGICAL PATTERN ORIENTATION DURING LIGHT-MEDIATED SYNTHESIS OF NANOSTRUCTURED SE-TE FILMS

Carim, A. I.; Batara, N. A.; Premkumar A.; Atwater, H. A.; Lewis, N. S. *ACS Nano*, **2016**, *10*, 102-111. DOI: 10.1021/acsnano.5b05119

4.1 Introduction

In this chapter, we investigate the patterns generated in photoelectrochemically grown Se-Te films utilizing two light sources with unique linear polarizations to understand the material growth response to the tailored excitation, as well as to identify strategies for obtaining morphology control and for generating three-dimensional morphological complexity. Films were generated using two same-wavelength sources with an array of polarization vector pairs as well as intensity ratios, and with two orthogonally polarized different-wavelength sources that had a series of intensity ratios. Computational modeling of the light-material interactions during photoelectrochemical growth successfully reproduced experimentally observed morphologies. Additional modeling of light scattering at the active film-solution interface, as well as simulations of light absorption idealized lamellar arrays, were also performed to understand the emergence of the morphologies generated using two discrete linear polarizations of light to drive film growth.

4.2 Results and Discussion

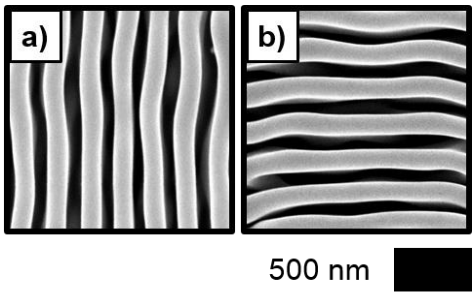

Figure 4.1. Effect of illumination source polarization on orientation of photoelectrodeposit morphology. SEMs representative of photoelectrodeposits generated with λ_{avg} = 630 nm illumination polarized (a) vertically and (b) horizontally.

Figure 4.1 presents representative SEMs of Se-Te photoelectrodeposits generated using illumination with a narrowband LED with λ_{avg} = 630 nm polarized vertically (a) and horizontally (b). In both cases, a highly anisotropic, lamellar-type morphology was observed. The long axis of the lamellar structures was oriented parallel to the polarization of the illumination; hence, vertical polarization resulted in vertically oriented lamellae whereas horizontal polarization yielded horizontally oriented lamellae.

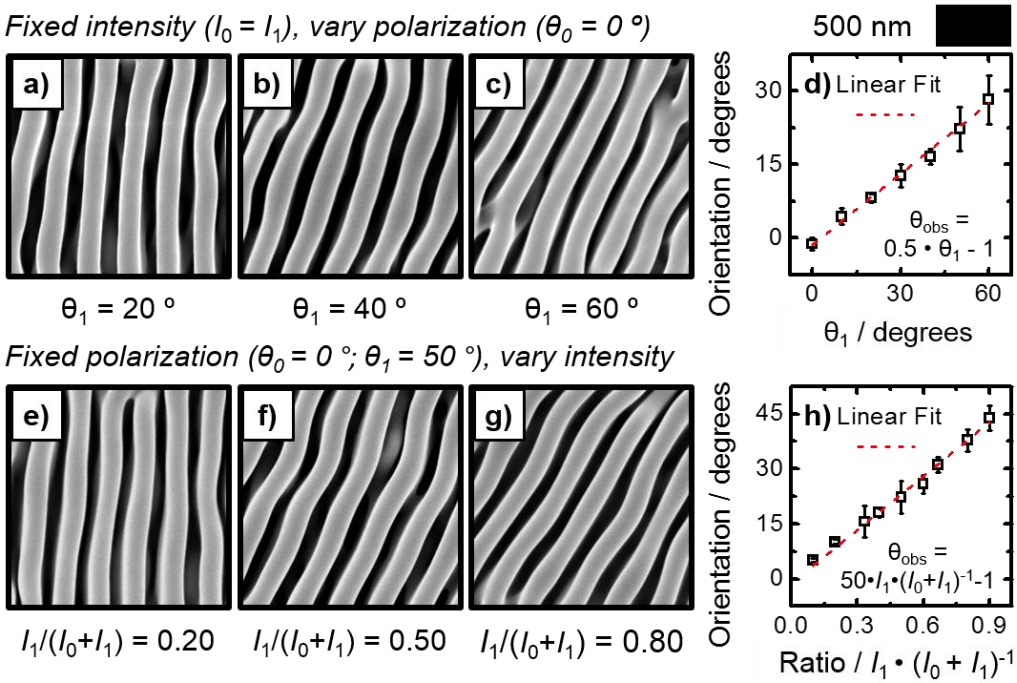

Figure 4.2. Orientation of photoelectrodeposit morphologies generated using two same-wavelength sources with differing linear polarizations. (a)-(c) SEMs representative of photoelectrodeposits generated using two λ_{avg} = 630 nm sources with equal intensity, the first source polarized vertically (θ_0 = 0 °) and the second at the indicated rotation (θ_1) clockwise from the vertical. (d) Plot of the rotation of the orientation of the long axis of the pattern (θ_{obs}) measured clockwise from the vertical as a function of θ_1. (e)-(g) SEMs representative of photoelectrodeposits generated using two λ_{avg} = 630 nm sources, each with a fixed linear polarization (the first polarized vertically, the second offset θ_1 = 50 ° clockwise from the vertical) with the indicated fraction of the total intensity supplied by the second source [I_1 / (I_0 + I_1)]. (h) Plot of θ_{obs} as a function of the fraction of the total intensity supplied by the second source.

Figure 4.2(a)-(c) presents SEMs representative of photoelectrodeposits generated using two equal intensity LED sources with λ_{avg} = 630 nm. One source was polarized vertically and the polarization of the second source was offset clockwise from the vertical by θ_1 = 20 ° (a), 40 ° (b), or 60 ° (c). In each case, a lamellar pattern

was observed that was similar to the pattern produced when only a single source was utilized. The long axis of the lamellar structures rotated clockwise away from the vertical in each case, and the magnitude of this rotation (θ_{obs}) increased with increasing values of θ_1. For θ_1 = 20 °, 40 °, and 60 °, values of θ_{obs} of 8 ± 1 °, 17 ± 2 °, and 28 ± 5 °, respectively, were measured. Figure 4.2(d) presents a plot of the observed magnitude of the pattern rotation from the vertical (θ_{obs}) as a function of θ_1. The trend was well-fit by a line of the form $\theta_{obs} = 0.5 \bullet \theta_1 - 1$. Figure 4.2(e)-(g) presents SEMs representative of photoelectrodeposits that were generated in a manner similar to those presented in Figure 4.2(a). Here, θ_1 was fixed to a value of 50 °, and the ratio of the intensity of this second source to the total intensity, $[I_1 / (I_0 + I_1)]$, was adjusted to 0.20 (e), 0.50 (f), and 0.80 (g), respectively. Again, the long axes of the lamellar structures were rotated clockwise away from the vertical in each case, and the magnitude of this rotation (θ_{obs}) increased with increasing values of the quantity $I_1 / (I_0 + I_1)$. For $I_1 / (I_0 + I_1)$ = 0.20, 0.50, and 0.80, values of θ_{obs} of 10 ± 1 °, 23 ± 5 °, and 38 ± 3 °, respectively, were observed. Figure 4.2(h) presents a plot of θ_{obs} as a function of the quantity $I_1 / (I_0 + I_1)$. The trend was well-fit by a line of the form $\theta_{obs} = 0.5 \bullet I_1 / (I_0 + I_1) - 1$.

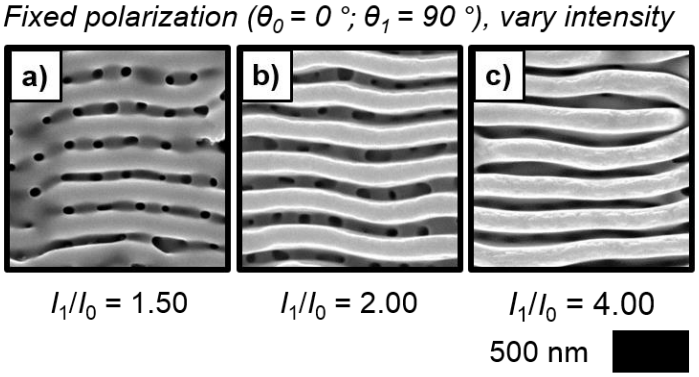

Figure 4.3. Photoelectrodeposit morphologies generated using orthogonally polarized same-wavelength sources. (a)-(c) SEMs representative of photoelectrodeposits generated using two λ_{avg} = 630 nm sources, one polarized vertically and the other horizontally, with the indicated intensity ratio between the horizontally and vertically polarized sources (I_1/I_0).

Figure 4.3 presents SEMs representative of photoelectrodeposits that were generated using two LED sources with λ_{avg} = 630 nm, with one source polarized vertically with intensity I_0 and the other polarized horizontally with intensity I_1, wherein $I_0 \neq I_1$. The intensity ratio between the horizontally polarized source and the vertically polarized source (I_1 / I_0) was 1.50 (a), 2.00 (b), and 4.00 (c). In (a), a square mesh morphology was observed in which a lamellar pattern was produced with the long axes of the lamellae running horizontally, superimposed over another similar pattern in which the long axes of the lamellae ran vertically. The contrast in the SEM suggests that the vertically aligned lamellae were shorter (darker) than those running horizontally. The pattern in (b) is similar to that in (a) but the horizontally oriented lamellae appeared to increase in height relative to the lamellae that ran vertically. In (c) only horizontally running lamellae are visible, and the contrast in the SEM does not suggest the formation of any other structure.

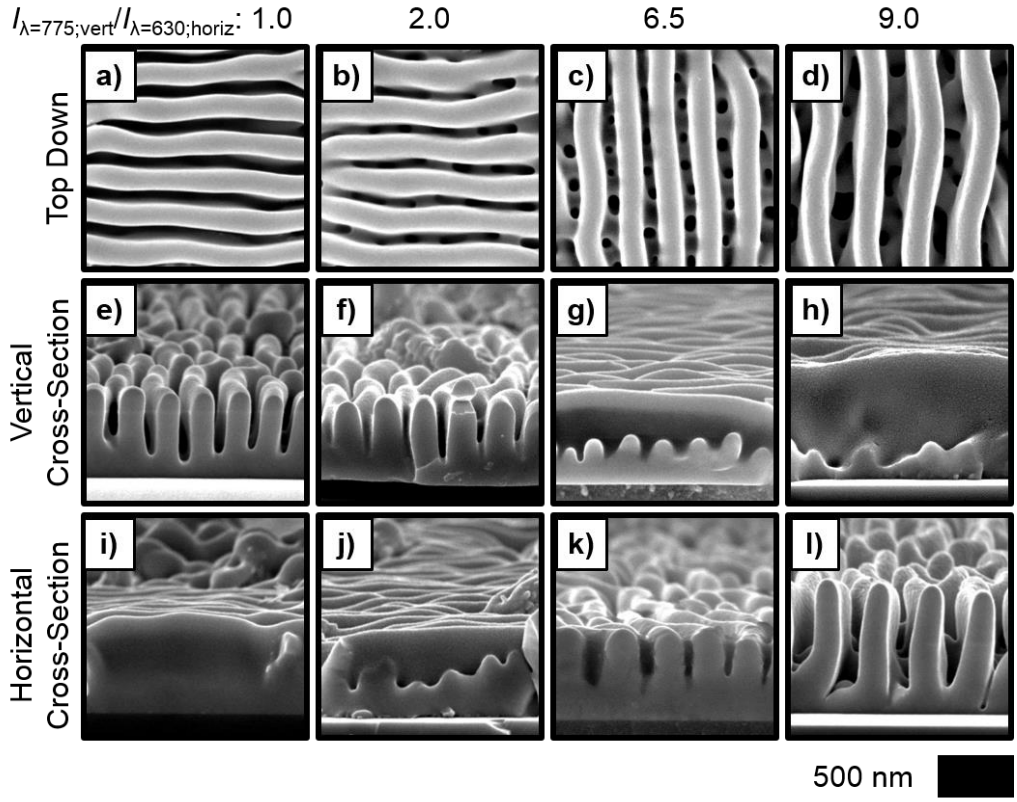

Figure 4.4. Photoelectrodeposit morphologies generated using orthogonally polarized sources with differing wavelengths. (a)-(d) Representative SEMs acquired in plan view of photoelectrodeposits generated using simultaneous illumination from a horizontally polarized λ_{avg} = 630 nm source and a vertically polarized λ_{avg} = 775 nm source with the indicated intensity ratio between the sources ($I_{\lambda=630;horiz}$ / $I_{\lambda=780;vert}$). (e)-(f) Same as (a)-(d) but cleaved along the vertical axis (perpendicular to the polarization of the λ_{avg} = 630 nm illumination) and acquired in cross-section. (i)-(l) Same as (a)-(d) but cleaved along the horizontal axis (perpendicular to the polarization of the λ_{avg} = 775 nm illumination) and acquired in cross-section.

Figure 4.4(a)-(d) presents a series of top down SEMs that are representative of photoelectrodeposits generated using simultaneous illumination with a LED source with λ_{avg} = 775 nm polarized vertically and a LED source with λ_{avg} = 630 nm polarized horizontally, with intensity ratios between the two sources ($I_{\lambda=775;vert}$ / $I_{\lambda=630;horiz}$) of 1.0

(a), 2.0 (b), 6.5 (c), and 9.0 (d), respectively. In (a), a lamellar structure was observed in which the long axes of the lamellae were oriented horizontally. The SEM in (b) is similar to that in (a) but displays a small amount of contrast in the spaces between the horizontally running lamellae. In (c), a lamellar structure in which the long axes of the lamellae are oriented vertically is observed. This structure exhibited a larger periodicity than those in (a) and (b). Also, vertically periodic contrast was observed in the space between the lamellae, suggesting the presence of a second set of intersecting lamellae having long axes oriented along the horizontal direction. In (d), like (c), a lamellar structure in which the long axes of the lamellae were oriented vertically was observed, and again the periodicity of this structure was greater than that observed in (a) or (b). Some contrast is visible in the spaces between the vertically running lamellae, but unlike in (c) this contrast did not appear to be periodic. Figure 4.4(e)-(h) and (i)-(l), respectively, present SEMs acquired from the same samples as in (a)-(d), but acquired in cross-sectional view by cleaving the substrate and film along the vertical (perpendicular to the polarization vector of the λ_{avg} = 630 nm illumination during growth), and along the horizontal (perpendicular to the polarization vector of the λ_{avg} = 775 nm illumination during growth), respectively. The cross-sections in (e) and (f) depict horizontally oriented lamellae similar to those seen in (a) and (b) from a perspective looking down the lamellar axes. In (g), a shorter, less well-defined structure similar to those observed in (e) and (f) and with a similar periodicity was observed superimposed on a mostly featureless ridge that is the side of a vertically running lamella similar to those observed in the top down micrograph in (c). In (h), the micrograph reveals a ridge that is also the side of a vertically running lamella, as in (g).

Some superimposed growth is again observed, with a varying height from left to right across the micrograph. In (i), the micrograph reveals a ridge that is the side of a horizontally running lamella similar to those presented in the top down micrograph in (a). In (j), a ridge similar to that observed in (i) is displayed. Superimposed on this ridge is growth with periodically varying height from left to right across the micrograph. The cross-sections in (k) and (l) depict vertically oriented lamellae similar to those seen in (c) and (d), from a perspective looking down the lamellar axes.

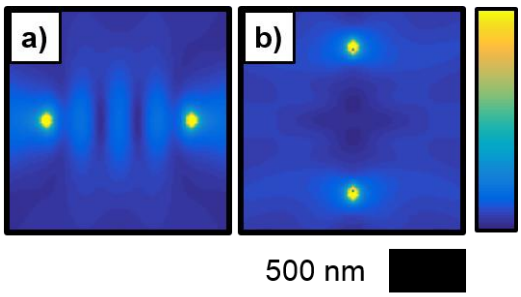

Figure 4.5. Normalized time-average of electric field magnitude from two dipoles emitting radiation with the same wavelength as a function of separation geometry. Dipoles are emitting radiation with a free space wavelength of λ = 630 nm in a medium of index n = 1.33 and are separated by a distance of two wavelengths in the direction (a) perpendicular and (b) parallel to the oscillation axis.

Point dipole radiation sources were used to model the amplitude modulation of the electric field at the active film-solution interface during photoelectrochemical growth that was caused by the inherent surface roughness of the deposited film. The time-averaged field amplitude resulting from two coherent dipole sources was calculated using two-dimensional FDTD simulations. Figure 4.5 presents the normalized time-average of the electric-field magnitude from two dipoles emitting

radiation with a free-space wavelength of $\lambda = 630$ nm in a medium of index $n = 1.33$ wherein the dipoles are separated by a distance of two wavelengths. In (a), the dipoles are separated perpendicular to the oscillation axis, and from left to right three strong vertically running interference fringes were observed in the area between the dipoles. In (b), the dipoles are separated parallel to the oscillation axis, and constructive interference between the dipoles was not observed.

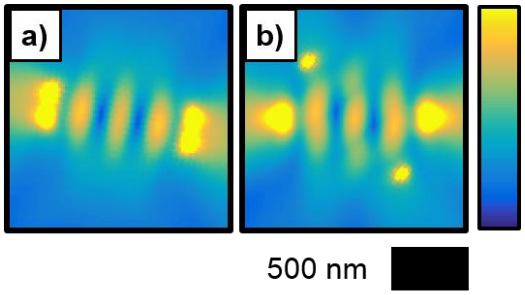

Figure 4.6. Normalized time-average of electric field magnitude resulting from two incoherently summed sets of dipole pairs each aligned perpendicular to a direction of oscillation. Dipoles are emitting radiation with a free space wavelength of $\lambda = 630$ nm in a medium of index $n = 1.33$. (a) One dipole set separated by two wavelengths along the horizontal axis and the axis of separation of the other set is rotated $\theta = 20$ ° clockwise from the horizontal, and both sets emit radiation with equal intensity. (b) One dipole set separated by two wavelengths along the horizontal axis and the axis of separation of the other set is rotated by $\theta = 50$ ° clockwise from the horizontal, and the two sets emit radiation with relative intensity $I_{\text{rotated}} / (I_{\text{rotated}} + I_{\text{horizontal}}) = 0.2$.

Figure 4.6 presents simulations similar to those in Figure 4.5 but with two incoherently summed sets of coherent dipole pairs aligned perpendicular to a direction of oscillation. In (a), one dipole set is separated along the horizontal axis while the axis of separation of the other is rotated $\theta = 20$ ° clockwise from the horizontal, and both

sets emit radiation with equal intensity. Interference fringes similar to those displayed in Figure 4.5(a) were observed but were rotated clockwise from the vertical by θ_{obs} = 10 °. In (b), one dipole set is separated along the horizontal axis while the axis of separation of the other is rotated θ = 50 ° clockwise from the horizontal, and the two sets were simulated to emit radiation with a relative intensity $I_{rotated} / (I_{rotated} + I_{horizontal})$ = 0.2. Interference fringes similar to those in (a) were observed, and the most intense parts of the fringes were measured to be rotated clockwise from the vertical by θ_{obs} = 9 °.

Computer modeling of the photoelectrochemical growth process was performed to analyze the morphologies expected for films generated as a result of the fundamental light-matter interactions during the deposition, using simultaneous illumination with two same-wavelength sources having different linear polarizations. The two-step, iterative model described in Chapter 1 was utilized wherein electromagnetic simulations were first used to calculate the local photocarrier-generation rates at the electrode/solution interface and then electrochemical addition of mass was simulated via a Monte Carlo method that utilized the local photocarrier-generation rate to weight the local probabilities of mass. During the early stages of deposition, dipole sources could be used to represent point-like scattering features due to surface roughness of the deposit and help to visualize the periodic absorption profile that occurs between two scattering features along the growth front. However, at later times, these interfacial features evolved into anisotropic structures that had an extended spatial structure. Utilization of the modeling algorithm, which recalculated the scattering and absorption profile as the film morphology evolved, enabled the

growth process to be fully reproduced. The model both incorporated the absorption modulation resulting from surface roughness during the early stages of growth and also captured the dynamic feedback between light absorption and material growth which resulted in 3D structures that agreed with experiment.

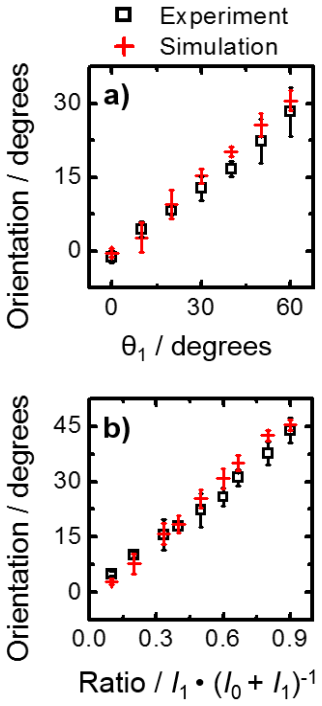

Figure 4.7. Orientation of photoelectrodeposit morphologies generated using two same-wavelength sources with differing linear polarization derived computationally from growth modeling compared to experimental results. (a) Plot of the orientation of the pattern long-axis (θ_{obs}) measured clockwise from the vertical as a function of the polarization orientation of one source (θ_1) for two-source illuminated photoelectrodepositions with same-wavelength (λ_{avg} = 630 nm), equal intensity sources when the other source was polarized vertically (θ_0 = 0 °). (b) Plot of θ_{obs} as a function of the fraction of the total intensity [I_1 / (I_0 + I_1)] delivered by a source polarized linearly θ_1 = 50 ° clockwise from the vertical in two-source illuminated photoelectrodepositions with same-wavelength sources when the other source was polarized vertically.

The experiment described in Figure 4.2(a)-(d) was simulated, wherein two equal intensity sources with λ_{avg} = 630 nm were utilized and one source was polarized vertically while the polarization of the second source was offset clockwise from the vertical by θ_1, and the observed rotation of the long-axis of the lamellar pattern clockwise away from the vertical (θ_{obs}) was derived. Figure 4.7(a) presents a plot of both the experimentally and computationally derived values of θ_{obs} as a function of θ_1. The experiment described in Figure 4.2(e)-(h) was also simulated, wherein the two sources with λ_{avg} = 630 nm were again utilized, with one source polarized vertically and the other at $\theta_1 = 50\,°$ from the vertical in the clockwise direction, while the fraction of the total intensity delivered by the second source [$I_1 / (I_0 + I_1)$] was varied. Figure 4.7(b) presents a plot of both the experimentally and computationally derived values of θ_{obs} for this experiment as a function of [$I_1 / (I_0 + I_1)$]. For both experiments, the empirically and computationally derived values of θ_{obs} were in good agreement, and were linear functions of either θ_1 or [$I_1 / (I_0 + I_1)$].

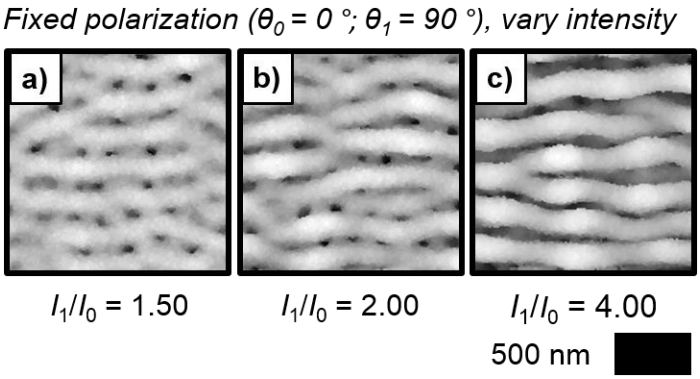

Figure 4.8. Simulated photoelectrodeposit morphologies generated using orthogonally polarized same-wavelength sources. (a)-(c) Simulated morphologies generated using two λ_{avg} = 630 nm sources, the first polarized vertically and the second horizontally, with the indicated intensity ratio between the horizontally and vertically polarized sources (I_1/I_0).

Additionally, computer modeling of the growth process was also performed to simulate the morphologies expected for films generated using simultaneous illumination from two orthogonally polarized, same-wavelength sources with unequal intensities. The experiment described in Figure 4.3(a)-(c) was modeled (Figure 4.8), wherein two unequal intensity sources with λ_{avg} = 630 nm were utilized with one source polarized vertically and the other horizontally. The intensity ratio between the horizontally polarized source and the vertically polarized source (I_1 / I_0) was 1.50 (a), 2.00 (b), and 4.00 (c), respectively. The simulated morphologies were in close accord with those observed experimentally (Figure 4.3), producing a square mesh morphology wherein the horizontally oriented lamellae were taller than those oriented vertically for I_1 / I_0 = 1.50 and 2.00, and producing a single, horizontally oriented lamellar morphology for I_1 / I_0 = 4.00.

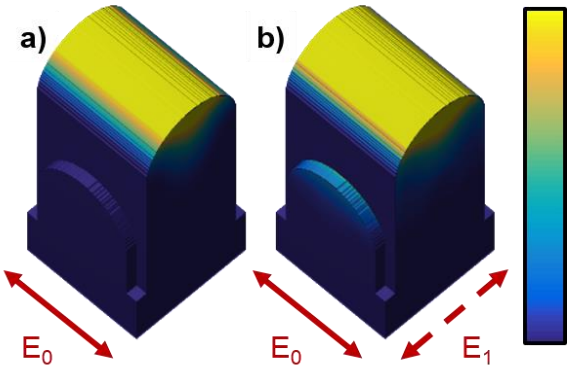

Figure 4.9. Computational analysis of light absorption in idealized models of structures generated via photoelectrodeposition using orthogonally polarized same-wavelength sources. (a) Simulated power absorption of two idealized, orthogonal lamellae under λ = 630 nm plane wave illumination polarized parallel to the taller feature (E_0). The width of each structure is typical of lamellar structures generated via photoelectrodeposition with λ_{avg} = 630 nm illumination and the length of each lamella is typical of one period of such structures. (b) Same as (a) but with the addition of a second λ = 630 nm source with 0.5 times the intensity of the first and polarized perpendicular to the taller feature (E_1) (sources assumed to be incoherent).

To further understand the growth of the morphologies that were observed when two orthogonally polarized sources of differing intensities and/or wavelengths were utilized, three sets of simulations of light absorption in idealized intersecting lamellar features were performed. First, films that had been experimentally photoelectrodeposited under vertically polarized λ_{avg} = 630 nm illumination alone and 775 nm illumination alone were analyzed using SEM to derive the lamellar periods and widths of the resultant structures. These values were then used as the inputs for the lengths and widths of the idealized structures. Two idealized lamellae were oriented so as to intersect at a 90 ° angle and were assigned heights of 200 nm and 400 nm. In the first set of simulations, designed to help understand the growth of the morphologies

that were observed when two orthogonally polarized sources with the same wavelength were used (λ_{avg} = 630 nm; Figure 4.3), the two lamellae both had widths that corresponded to the width of the lamellar structures observed for deposition with λ_{avg} = 630 nm illumination alone, and both had lengths equal to the corresponding lamellar period. Figure 4.9 presents the power absorption profile calculated (a) from a single λ = 630 nm plane wave source polarized parallel to the long axis of the taller lamella and (b) from two λ = 630 nm plane wave sources wherein one source was polarized parallel and the other perpendicular to the long axis of the taller lamella, with the source polarized perpendicular having half the intensity of the one polarized parallel. Figure 4.9(a) shows that significant absorption was observed only near the tip of the taller lamella. Figure 4.9(b) indicates that absorption was observed both at the tip of the taller lamella as well as at the tip of the shorter lamella.

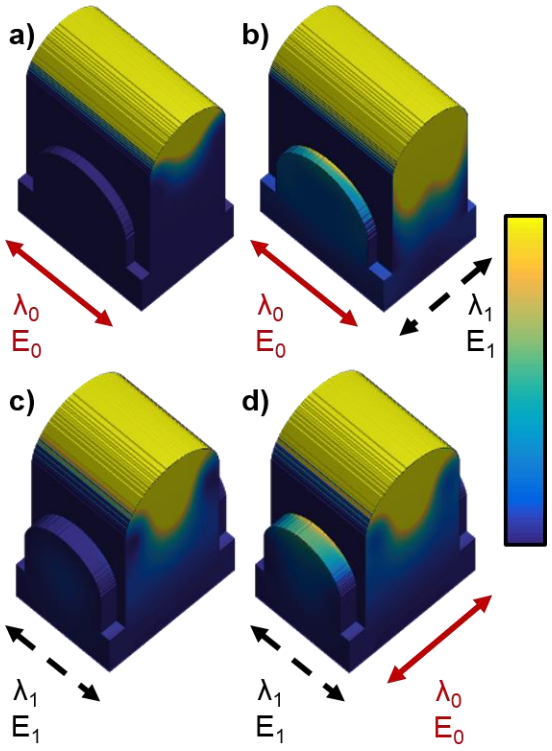

Figure 4.10. Computational analysis of light absorption in idealized models of structures generated via photoelectrodeposition using orthogonally polarized sources with differing wavelengths. (a) Simulated power absorption of two ideal orthogonal lamellae under λ_0 = 630 nm plane wave illumination polarized parallel to the taller feature (E_0). The width of the taller structure is typical of lamellar structures generated via photoelectrodeposition with λ_{avg} = 630 nm illumination whereas the width of the shorter structure is typical of the structures generated with λ_{avg} = 775 nm illumination. (b) Same as (a) but with the addition of a λ_1 = 775 nm plane wave source with twice the intensity of the λ_0 = 630 nm source and polarized perpendicular to the taller feature (E_1) (sources assumed to be incoherent). (c) Simulated power absorption of two ideal orthogonal lamellae under a λ_1 = 775 nm plane wave source polarized parallel to the taller feature (E_1). The width of the taller structure is typical of lamellar structures generated via photoelectrodeposition with λ_{avg} = 775 nm illumination whereas the width of the shorter structure is typical of the structures generated with λ_{avg} = 630 nm illumination. (d) Same as (c) but with the addition of a λ_0 = 630 nm plane wave source 6.5 times less intense than the 775 nm source and polarized perpendicular to the taller feature (E_0) (sources assumed to be incoherent).

The second and third sets of light absorption simulations were designed to help understand the generation of the morphologies observed when two orthogonally polarized sources with λ_{avg} = 630 nm and λ_{avg} = 775 nm were utilized simultaneously (Figure 4.4). In the second set of simulations, the taller lamellar feature had a width corresponding to the width of the lamellar structures observed for deposition with λ_{avg} = 630 nm illumination alone, and the length of the shorter lamella was equal to the corresponding lamellar period. The shorter lamellar feature had a width corresponding to the width of the lamellar structures observed for deposition with λ_{avg} = 775 nm illumination alone, and the length of the taller lamella was equal to the corresponding lamellar period. Figure 4.10(a) and (b), respectively, present the power absorption profile calculated from a single λ = 630 nm plane-wave source polarized parallel to the long axis of the taller lamella alone, and from the same source as in (a) as well as a secondary λ = 775 nm plane-wave source polarized perpendicular to the long axis of the taller lamella that was twice as intense as the λ = 630 nm source. In Figure 4.10(a), significant absorption was observed only near the tip of the taller lamella. In Figure 4.10(b), absorption was observed both at the tip of the taller lamella as well as at the tip of the shorter lamella. The third set of simulations utilized lamellar structures having similar dimensions as the second set but with the heights of the two lamellae exchanged. Figure 4.10(c) and (d), respectively, present the power absorption profile calculated from a single λ = 775 nm plane-wave source polarized parallel to the long axis of the taller lamella alone, and from the same source as in (c) as well as a secondary λ = 630 nm plane wave source polarized perpendicular to the long axis of the taller lamella that was 6.5 times less intense than the λ = 775 nm source. As with

the second set of simulations (Figure 4.10(a)-(b)) in Figure 4.10(c) significant absorption was observed only near the tip of the taller lamella, whereas in Figure 4.10(d) absorption was observed both at the tip of the taller lamella as well as at the tip of the shorter lamella.

When two sources having the same wavelength (λ_{avg} = 630 nm) but having differing, linear, non-orthogonal polarizations were utilized simultaneously (Figure 4.2(a)-(c) and (e)-(g)), a lamellar pattern identical to those observed with only a single source (Figure 4.1) was observed, except for an in-plane rotation. This result can be readily understood because any linear polarization can be equivalently expressed as the sum of two orthogonal linear polarizations, e.g. vertical and horizontal. Thus, no difference may be observed between the morphology generated if a single illumination source is utilized relative to the morphology generated if two sources are used simultaneously, as long as the intensity-weighted average of the polarization orientations of the two tandem sources is the same as the polarization of the single source. The experimental data quantitatively supports this hypothesis, because the observed orientation of the pattern (θ_{obs}) for the two-source experiments was almost exactly equal to the intensity-weighted average polarization orientation: ($I_0 \bullet \theta_0 + I_1 \bullet \theta_1$) / ($I_0 + I_1$). For the experiment wherein the intensity of the sources was equal ($I_0 = I_1$), the first source was polarized vertically ($\theta_0 = 0$ °) and the angle between the polarization vectors (θ_1) was varied, θ_{obs} would be expected to have the form $0.5 \bullet \theta_1$. This expectation is very close to the experimentally observed relation of $\theta_{obs} = 0.5 \bullet \theta_1 - 1$. Similarly, for the experiment in which the polarizations of the two sources were fixed ($\theta_0 = 0$ ° and $\theta_1 = 50$ °) and the relative contribution of the two sources to the

total intensity was varied, θ_{obs} would be expected to have the form $50 \bullet [I_1 / (I_0 + I_1)]$, which again is very close to the experimentally observed relation of $\theta_{obs} = 50 \bullet [I_1 / (I_0 + I_1)] - 1$. The difference between the expected and experimentally observed relations for θ_{obs}, a -1 ° offset, is likely a minor systematic error arising from a minor calibration error in a polarizer setting. This notion is supported by the facts that a value of $\theta_{obs} = -1 \pm 1$ ° was observed when $\theta_0 = \theta_1 = 0$ °, and that the experimentally observed values of θ_{obs} were generally marginally lower than expected.

The quantitative agreement between the values of θ_{obs} measured in the experiments using same-wavelength (λ_{avg} = 630 nm) sources with mutually different linear, non-orthogonal polarizations simultaneously, and in the analogous computer simulations (Figure 4.7), which utilized minimal empirical data, for all investigated conditions, suggests that the empirically observed behavior is the result of a fundamental optical phenomenon. This notion is supported by the results of the dipole scattering simulations (Figure 4.5 and 4.6). The interference fringes observed between two simulated radiation-emitting dipoles separated along the horizontal axis, and perpendicular to the oscillation axis, (Figure 4.5(a)) are reminiscent of the lamellar morphology observed in the photoelectrodeposit generated with vertically polarized illumination (Figure 4.1(a)), and have been hypothesized to promote the initial growth of this periodic and anisotropic structure by providing the necessary spatially varying distribution of light intensity.[47] When two sets of dipoles were simulated with some angle, θ, between their axes of separation, the resultant interference fringes were observed to rotate by an angle, θ_{obs}, that is in good agreement with relation of $\theta_{obs} = \theta \bullet [I_{rotated} / (I_{rotated} + I_{horizontal})]$. Thus, the dipole scattering simulations suggest that the

orientation of the lamellar structures in the non-orthogonal, same-wavelength experiments is a manifestation of the elementary phenomenon of superposition of waves.

When two orthogonally polarized same-wavelength (λ_{avg} = 630 nm) sources that had unequal mutual intensities were utilized, the resultant structures appeared to consist of two intersecting sets of orthogonally oriented lamellae wherein the relative heights of each set of lamellae were directly proportional to the relative source intensities (Figure 4.3). These observations indicate that the utilization of orthogonally polarized sources can enable independent control over different features of the resultant film morphology, and thus comprises a potentially useful tool for generating application-specific structures. The reproduction of the experimental morphologies by the growth model (Figure 4.8) suggests that the generation of the intersecting structures when orthogonally polarized light is used is a result of the intrinsic light-matter interactions that occur during the deposition process. Moreover, the continued growth of such intersecting structures under the aforementioned conditions is consistent with the simulations of light absorption in the idealized versions of the structures (Figure 4.9) wherein illumination from two orthogonally polarized sources is preferentially absorbed in the tips of both structures. These areas represent the photoelectrochemical growth fronts: preferential light absorption in these areas supports continued anisotropic growth in a manner that preserves the cross sections of the features. Furthermore, visualization of the difference in the absorption profile with and without the contribution from the source parallel to the shorter feature

indicated that this source was solely responsible for absorption along the shorter feature.

Intersecting lamellar structures were also observed when two orthogonally polarized sources with differing wavelengths (λ_{avg} = 630 nm and 775 nm) were utilized. Again, the relative heights of each set of lamellae were proportional to the relative source intensities. However, for $I_{\lambda=775;vert} / I_{\lambda=630;horiz} = 1.0$, SEM analysis provided little evidence for the presence of periodic, anisotropic structures with long axes oriented along the vertical, and, for $I_{\lambda=775;vert} / I_{\lambda=630;horiz} = 2.0$, such structures were found to be shorter than the simultaneously observed, horizontally-oriented structures. Also, for $I_{\lambda=775;vert} / I_{\lambda=630;horiz}$ = 6.5 and 9.0, structures with horizontal periodicity were observed. These observations are consistent with previous physical characterization suggesting that lower rates of photoelectrodeposition may be observed when utilizing λ = 775 nm than when utilizing λ = 630 nm illumination.

Unlike the intersecting lamellar structures generated using two orthogonally polarized same-wavelength sources (λ_{avg} = 630 nm), when two orthogonally polarized sources with differing wavelengths (λ_{avg} = 630 nm and 775 nm) were used, the periodicities of two sets of lamellae were unequal. The set with their long axes oriented parallel to the polarization vector of the λ_{avg} = 775 nm source displayed a greater periodicity than those oriented parallel to the polarization vector of the λ_{avg} = 630 nm source. This difference in periodicity is a consequence of differing anisotropic light absorption profiles in the growing structures in response to the different wavelengths, and the lamellar period increases monotonically with λ.[47] Moreover, these results indicate that not only is it possible to control the relative heights of structures with

orthogonal periodicities, but also indicate that the magnitudes of those periodicities can also be controlled, which may be of use in the construction of purpose-designed structures. Simulations in idealized versions of these intersecting structures were again consistent with their growth (Figure 4.10): illumination polarized along the long axis of a lamellar structure (of the same wavelength used to generate that structure) is preferentially absorbed in the tip of that structure relative to light polarized perpendicularly (of a different wavelength).

Dynamic photoelectrochemical growth may find potential in the generation of nanophotonic optical elements including planar lenses and mirrors,[69-71] polarization-sensitive filters and photodetectors,[72] and nanostructured scaffolds.[73,74] The results described in this chapter have several implications for the use of this process to design application-targeted structures. First, controlling the pattern orientation with respect to the substrate does not require changing the polarization state of a single source, for example, rotating a linear polarizer. Instead, two sources could be used with static linear polarizations and the pattern orientation could be controlled by changing the relative intensity of the sources. Manipulating such a quantity continuously or in discrete steps over time could be used to generate morphological complexity. The utilization of orthogonal sources also presents another method to generate intricate structures wherein control of the feature size in three dimensions of two patterns may be obtained simultaneously and independently.

4.3 Conclusions

Nanopatterned Se-Te films were photoelectrochemically prepared using simultaneous illumination from two light sources with discrete linear polarizations. Films grown with two non-orthogonally polarized, same-wavelength sources displayed lamellar morphologies wherein the long axes of the structures were aligned along the intensity-weighted average polarization vector. Such behavior was consistent with simulations of light scattering at the solution-film interface at the onset of photoelectrochemical growth. Simulations of the growth with such illumination showed that the emergence of the observed morphologies could be understood by considering the fundamental light-matter interactions during deposition. Structures consisting of two sets of intersecting, orthogonal lamellae were generated when two orthogonally polarized illumination sources were utilized wherein the periodicity and feature size of each set of lamellae was proportional to the wavelengths of the illumination source polarized along their long axes. The evolution of such morphologies was consistent with simulations of light absorption in idealized intersecting lamellar structures, which indicated that the lamellae preferentially absorbed light polarized along with the electric field vector parallel to the long axes. The cumulative data suggest that under the conditions investigated, the morphology of the photoelectrodeposit is sensitive simultaneously to the polarization of both sources utilized during growth. Additionally, the use of such tailored optical excitation provides control over the pattern orientation and enables the generation of three-dimensional structures that cannot be produced with a single polarization.